Construction of Receive Arrays

21st ISMRM: Weekend Educational Course

Boris Keil
keil@nmr.mgh.harvard.edu

Introduction

In the last decade, parallel detection of the Magnetic Resonance Imaging (MRI) signal with multiple receive-only surface coils has proven valuable for increasing image sensitivity and acquisition speed. The success of parallel imaging methods has driven the design of MR receive arrays with an increasing number of elements [1–5]. The high degree of parallelism requires systemized design, construction and testing in order to implement the large number of tuned receive circuits with minimal mutual interaction and has altered the workflow for how we construct receive arrays [1].

The main aim of this course is to inform MRI researchers/students about the basic procedures for phased-array construction and describe an optimized protocol for constructing, tuning and decoupling a highly parallel array coil. The goal is to provide a better understanding of the basic experimental RF tools and procedures to facilitate the efficient design and construction of highly parallel MRI receive-arrays. We demonstrate the protocol with the construction of a 32-channel brain array of overlapped circular surface coil elements.

The course will go through the following steps for constructing a prototyped noncommercial array coil: *i*) the layout of the array elements, ii) creating and tuning a single loop element, *iii*) estimating the coil quality factor, *iv*) adjusting the single loop and match circuit to optimize preamplifier decoupling and *v*) active PIN diode detuning circuitry, *v*) placing the neighboring elements to allow them to be efficiently constructed and inductively decoupled, *vi*) assembling the array, *vii*) decoupling the array elements from one another, *viii*) tune and match the coil elements, and *iix*) performing final bench tests.

Part 1: Helmet Design

The helmet size was obtained from the surface contours of aligned 3D MRI scans from N=20 subjects. The helmet shape was taken by dilating the 95% contour to accommodate 3 mm foam padding. Using a 3D CAD program, the helmet was designed as a deep posterior segment covering all but the face and forehead so the child can lie down into the posterior coil section. A separate “frontal paddle” is then positioned over the forehead. This configuration simplifies the need to mate the two segments and avoids a single helmet which comes down over the head. It maintains an open area over the eyes and face. This coil design is an example of a sized-matched array to be used for 1-year-old children [6].

The helmet model is shown in Figure 1. The geometric structure of the coil element layout (see below) is engraved on the helmet as part of the CAD design (see Figure 1). Additionally, standoffs for the preamplifiers are included into the 3D design. The final design of the helmet parts and phantom were printed in acrylonitrile butadiene styrene (ABS) plastic using a rapid prototyping 3D printer.

Proc. Intl. Soc. Mag. Reson. Med. 21 (2013)

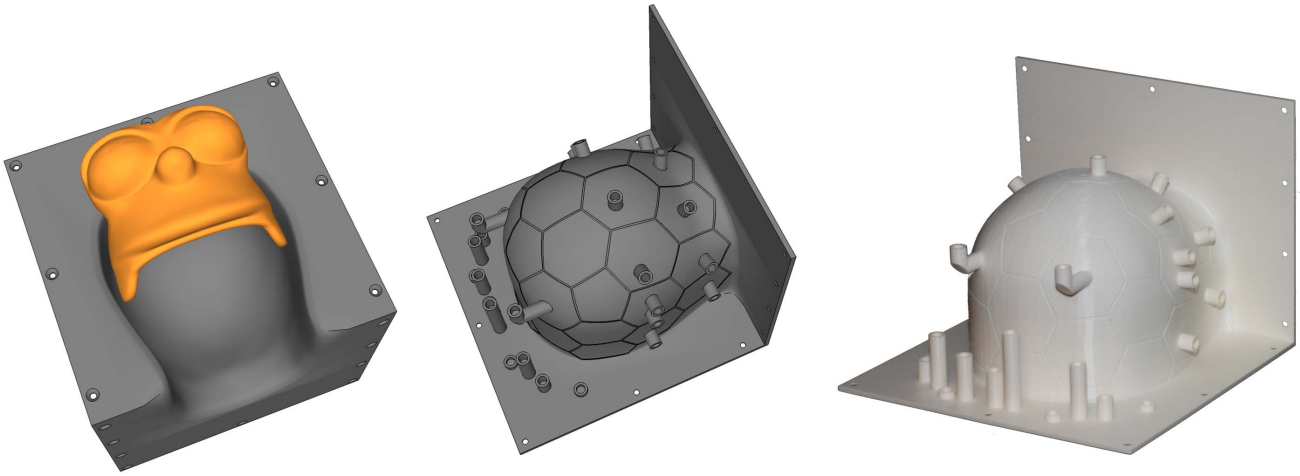

Figure 1: 3D CAD model of the coil former (*left, middle*) and 3D printed coil helmet (*right*).

Part2: Loop layout

Given the geometrical constraints of the helmet and knowledge of the extent of anatomical coverage desired, the next step is to layout the pattern of overlapping circular coils which geometrically "tile" this 2D space. We determine the tiling pattern using hexagons and pentagons (where each pentagon or hexagon represents a circular loop element) either in the CAD layout (see Figure 1) or by cutting the hexagons and pentagons from paper or cardboard and physically laying them out on the coil former. The goal is to completely tile the curved surface using these elements. One tile choice is to place one hexagon surrounded by six other hexagons; a pattern useful for tiling locally flat sections. Alternatively, a "soccer-ball" tiling pattern can be used with hexagons and pentagons (one pentagon surrounded by 5 hexagons) [7]. This soccer-ball pattern tiles a spherical space. Thus, the hexagonal pattern is useful for tiling flat sections of the body and the soccer-ball geometry is useful for adding local curvature. Given a helmet, we can then lay out a suitable combination of hexagon subsections and pentagon subsections adjusting the size appropriately to meet the desired number of channels. For the infant array under construction, the shape of the bottom part incorporated 25 hexagons and 3 pentagons. The anterior part (forehead paddle) completes the 32 channel with additional 4 overlapped elements.

Part2: Loop Design

The diameters of the loop coils corresponding to the pentagon/hexagon tiles on the helmet are determined from the size of the pentagon/hexagon tiles; the loop diameter is slightly larger than the diameter of the circle which inscribes the vertexes of the hexagon/pentagons. Next, we construct a pair of test loops to determine the values of the needed capacitors and fine-tune the final size for each coil element. We recommend that the researcher complete these test loops and validate them with imaging tests prior to completing the construction of the larger array.

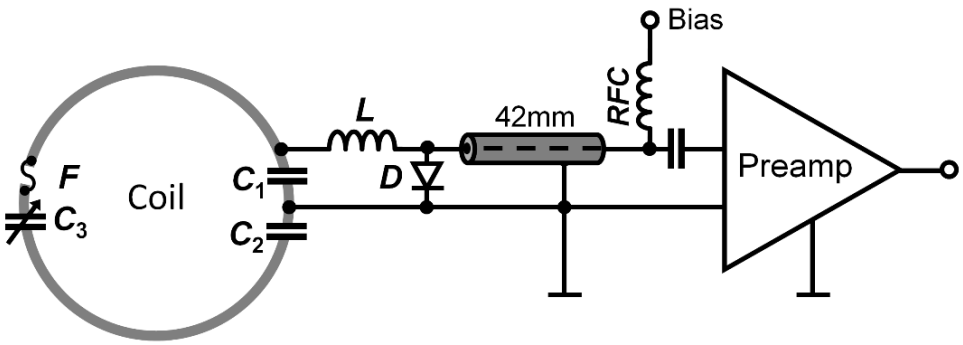

Figure 3: Circuit schematic for the coil element and preamp chain. In this case, the coil element comprises three capacitors: C_3 to adjust tuning and C_1 to provide impedance noise matched impedance (e.g. 50 Ohm). C_2 and C_1 have equal capacitance and provide a symmetrical circuit design. A detuning trap is formed around C_1 using variable inductor *L* and a diode *D*. If the detuning trap fails, an RF fuse *F* is inserted in the circuitry.

We used 16-awg thick tin-plated copper wire to form the loops with bridges to allow the coil conductors to cross-over one another without touching. We divided each loop symmetrically by two gaps where we place the capacitors (see schematic circuit in Figure 3, and photo in Figure 4). Thus, each half of the loop is joined at the top by the tuning capacitor and at the bottom by the output-circuit. These two sub-circuits are constructed on separate small circuit boards. The tuning capacitor circuit board contains a variable capacitor C_3 to fine-tune the loop resonance to 123.25 MHz and a series fuse *F* for passive protection against large currents potentially induced during transmit. Figure 4 shows the tuning of a single loop with a double probe S_{12} measure as well as the determination of the *Q* factor of the coil both alone and with the other elements in place (see Part 4). The output circuit-board (shown in detail in the photo of Figure 5) contains a capacitive voltage divider (C_1, C_2) to match the elements output to the impedance, $\underline{Z}_{NM}$, desired by the preamplifier[8] (Siemens Healthcare, Erlangen Germany) for an optimized noise match (e.g. 50 Ohm). The drive-point circuit board also incorporates an active detuning circuit across the match capacitor. The active detuning is achieved using a PIN diode *D* in series with a variable inductor *L*, which together with the match capacitor C_1 resonates at the Larmor frequency. Thus, when the PIN diode is forward biased (transmit mode), the resonant parallel LC_1 circuit inserts a high impedance in series with the coil loop, blocking current flow at the Larmor frequency during transmit.

Part 3: Coil quality factor

After the determination of the loop sizes and needed components, we calculate the coil quality factor (*Q*), which describes how much the reactive impedance dominates over the resistive impedance in the loop coil. It informs us of the power dissipated in loss mechanisms relative to the energy stored in the tuned circuit. Under sample-loaded conditions, the resistive impedance is the sum of the coil and sample resistances. We measure the ratio of the coil quality factor in terms of an unloaded (Q_{unload}) and a loaded coil (Q_{load}). We measure the ratio of Q_{unload} and Q_{load} for both a single loop element and a loop under test surrounded by its six non-resonant neighboring elements. The latter case informs us about the losses in the copper in nearest neighboring elements [2,9]. The procedure for measuring the *Q* of the loops using a loosely coupled double probe is shown in Figure 4. Care is taken that the probes are not too close to the loop under test (and thus perturbing the measurement) and that conductive material (such as tools and solder) is removed from the area during the test.

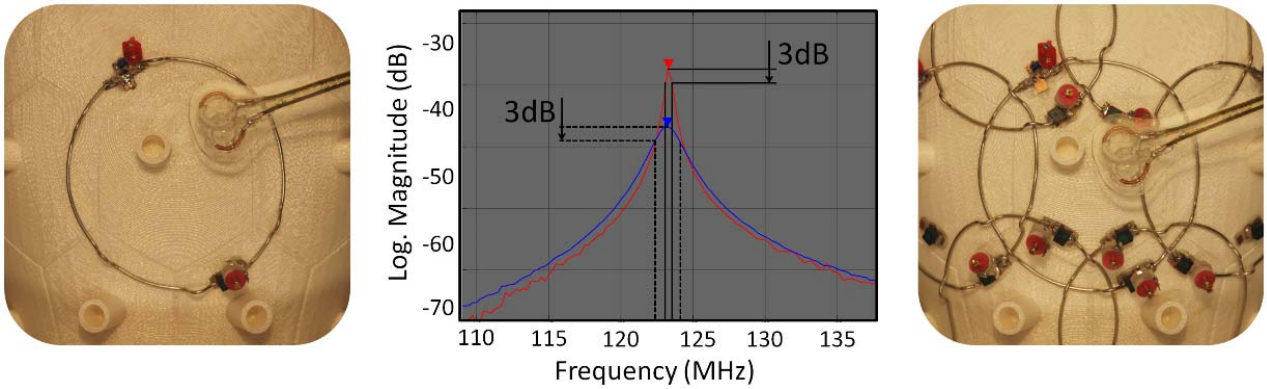

Figure 4: Measurement of the Ratio of $Q_{unloaded}$ to Q_{load}: All the estimations of *Q*-ratios should be done for both; a single loop (*left*) and a loop under test surrounded by its six non-resonant neighboring elements (*right*). Usually, copper loading of adjacent elements reduces the unloaded Q. The coil quality factor is simply given by $Q=\nu_0/\Delta\nu$, where ν_0 is the center frequency and $\Delta\nu$ is -3dB bandwidth. It is important that the double probe location does not change during both of the above measurements. The graphic in the *middle*, shows Q_{unload} (red S_{21} measure) and Q_{load} (blue S_{21} measure) when the neighboring elements were present.

Part 4: Tuning the Active Decoupling

As described above, the trap LC_1 together with the PIN diode, detune the loop during transmit with the body RF coil. To test that the detuning is adequate, we measure first the tuning of the LC_1 circuit using a single pickup loop ("sniffer probe" marked in Figure 5 and Figure 11c) connected to a network analyzer S_{11} measurement as shown in Figure 5. This trap circuit tuning step is done without the main coil loop being tuned (variable capacitor was still missing) and with the PIN diode forward biased (conductive state). After initial tuning of the trap circuit with the small sniffer probe, we attach the variable capacitor C_3 to close the circuit of the main loop and tuned the coil to 123.25 MHz using a double probe controlled via the S_{21} measure (Figure 6). Holding the double probe on the same position, but actively switching the forward bias of the PIN diode on an off, we measure the loop response in the tuned and detuned state (Figure 6 *middle*). We expect the active detuning to produce S_{12} >35dB isolation between these two states (see Figure 6).

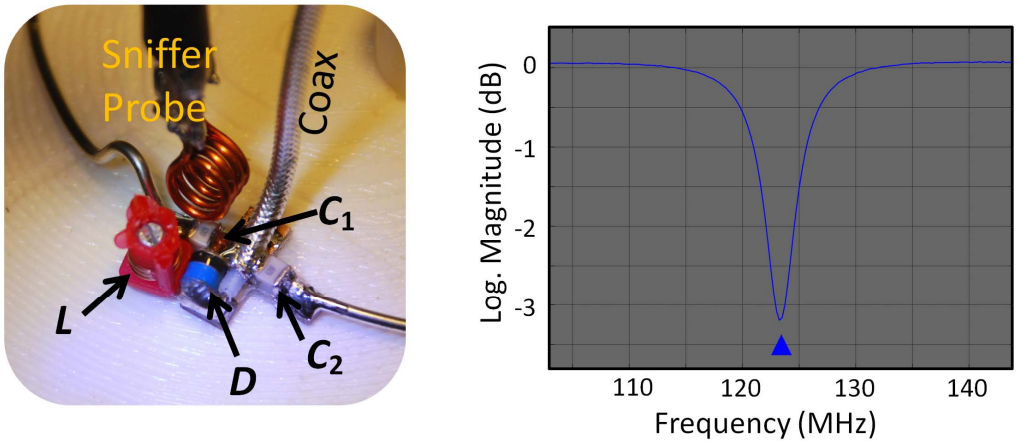

Figure 5: Pre-adjustment of the active detuning trap using a S_{11} measurement and a "sniffer" probe. The variable red inductor *L* and the match capacitor C_1 forms a parallel resonance circuit when the PIN diode *D* is forward biased in transmit mode. This spoils the *Q* of the coil element by providing a high series impedance and consequently blocking current flow at the Larmor frequency. Final results of an active detuned element is shown in Fig. 6.

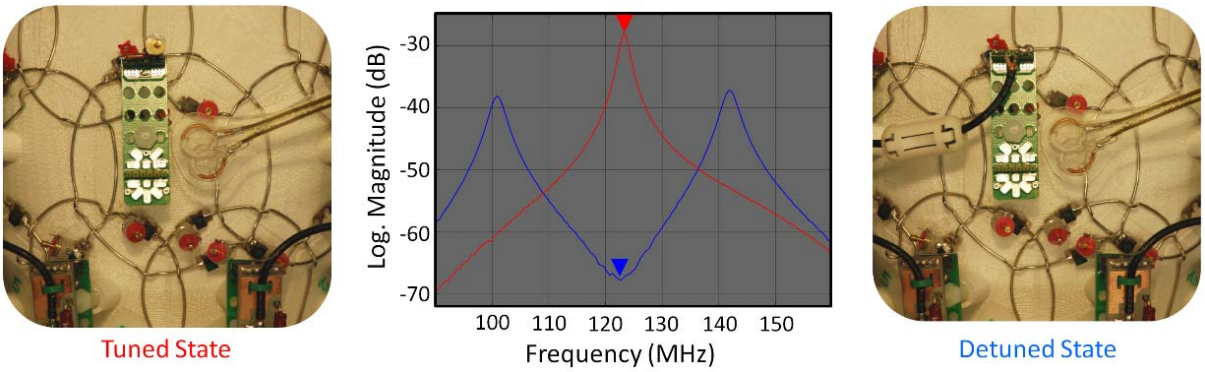

Figure 6: Measurement of active detuning. The S_{12} change was recorded for a given array element with and without forward bias current applied to the PIN diode trap. The difference of the two states determines the isolation between the receive array and the transmit coil. During the measurement of the tuning state (red trace), the preamplifier was replaced by a 50 Ohm dummy load (power matched). The constructed array shows an active detuning isolation of 40 dB.

Part 5: Preamplifier Decoupling

Preamplifier decoupling is used to reduce coupling between next-nearest and further neighbors. It has become one of the most important tools in constructing Rx arrays [10]. Optimization of the preamplifier decoupling is a critical step in constructing highly parallel arrays. The goal is to design the preamplifier/coil circuit so that the preamplifier performs a voltage measurement across the loop. Thus, the output circuitry (match + coax + preamplifier) forms a series high impedance in the tuned loop reducing current flow and thus reducing inductive coupling with other loop elements.

To transform the preamplifier's input impedance to a high series impedance in the loop, we first transforms this impedance (with short length coax cable and the given inductor L from the detuning trap) to a parallel inductance across the matching capacitor C_1 in the coil loop output. This parallel LC circuit is set to resonate at the Larmor frequency and introduces a high serial impedance in the coil loop. In this mode, minimal current flows in the loop and inductive coupling to other coils is minimized. This procedure is done by carefully controlling the cable length (42 mm in this case) between preamplifier and coil terminal.

We adjust the preamplifier decoupling viewing the S_{12} versus frequency for the coil in the tuned state (PIN diode reverse biased) with the preamp in place and powered on using the same decoupled double probe, but with reduced power output from the network analyzer (-25 dBm). It is important that the minimum of the S_{21} "dip" is at the Larmor frequency (Figure 7). Thus, verifying that the correct impedance transformation at the Larmor frequency was performed. Low-loss circuitry between the preamp input and the loop insures a high degree of preamplifier decoupling which can be indirectly measured by assessing the depth of the "dip" in Figure 7.

We are using a design, where the preamplifiers are mounted adjacent to each coil element to minimize losses between the inductive loop and the first stage of amplification. The close proximity between loop and preamp eliminates the need for a long cable between loop and preamplifier.

If a quantitative measure of the preamplifier decoupling is desired, the measurement can be repeated with the preamplifier replaced by a 50 Ohm load (or with the conjugate complex impedance $\underline{Z}^*_{NM}$ of the preamplifier's noise-match impedance $\underline{Z}_{NM}$., when a non-50-Ohm preamp is used). Then a comparison of the S_{12} at the Larmor frequency between the 50 Ohm terminated dummy load and the low impedance preamplifier quantifies the preamplifier decoupling [11].

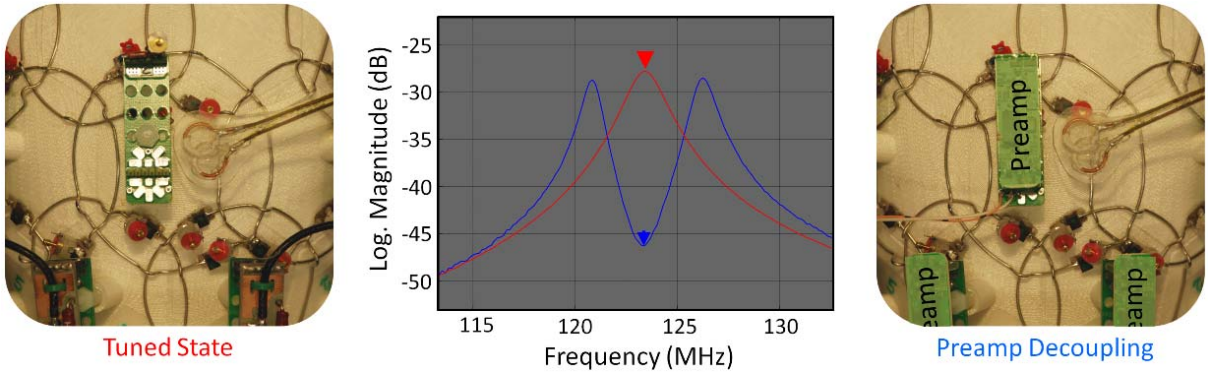

Figure 7: Preamplifier decoupling is estimated as the change in S_{21} measurement in the case of power match (red trace), which has the conjugate complex impedance of the coil impedance under load without the presence of the preamp (*left*) and the case of noise match (blue trace), which has termination by low impedance preamplifier (*right*). The difference between the two states (in dB) determines the preamp decoupling (*middle*). For simple checks that the preamplifier decoupling is occurring at the proper frequency, the noise match trace (red trace) is not needed, and a simple check that the dip in the noise matched (blue) trace occurs at the Larmor frequency. Since the noise matched trace is obtained with the preamplifier present, it can be verified on a completed array (with all covers and cabling) by detuning all but the coil under test using a coil plug test rig.

Part 6: Determining the Critical Overlap

In this step the overlap between neighboring elements is adjusted to null their mutual inductance [12]. Before performing this step, we must have completed the loop and active decoupling tuning of Part 3 for all loops on the helmet. We estimated the critical overlap ratio of a pair of loops by carefully moving those loops towards each other while measuring the S_{12} parameter between the tuned coils (with any other loops biased to the detuned state using their active decoupling circuit). We monitor the S_{12} interaction between the two neighboring coils using a test probe that plugs into the circuit board at the position of the preamplifier (see Figure 8).

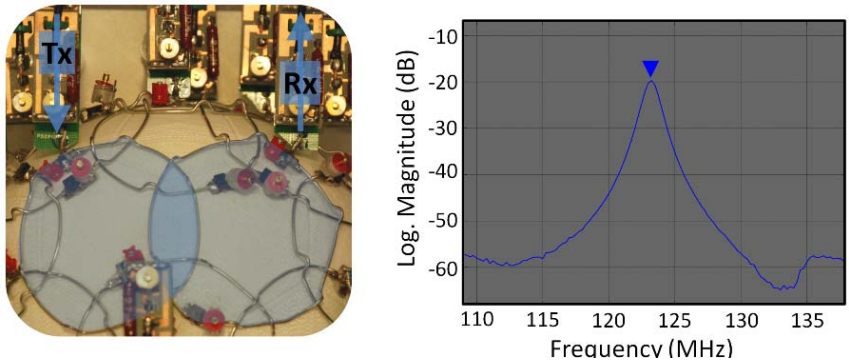

Figure 8: Adjustment and recording of the geometrical decoupling between two adjacent coil elements. When measuring the decoupling between an adjacent pair, all other unused elements of the array were detuned. Minimized coupling was achieved by empirically bending the crossing bridges on the loops. Coupling between nearest neighbor elements ranged from -15 dB to -21 dB with an average of -17 dB.

Part 7: Array Assembly

After successfully testing the first loops, we assemble the whole array: First, all the drive points and capacitor solder pads, made out of FR4 circuit material, are mounted on the helmet. Second, the 16-awg thick tin-plated copper wires are cut, bent and assembled over the whole array. Third, the preamplifier board including the 42 mm long coaxial cable were mounted to the designated holder (Figure 2), as well as wiring up the preamplifier and bias tee circuitry to the plug cables. All preamps were carefully orientated along the *z*-direction to minimize Hall effect issues [13–15]. Fourth, the detuning traps on the drive are adjusted to be resonant at the Larmor frequency when the PIN diode was forward biased, as described in Part 3.

Part 8: Geometrical Nearest-Neighbor Decoupling of the Array

The goal of the geometrical decoupling is to find a critical overlap of all adjacent coils in order to minimize the mutual decoupling between any pair of neighboring coils. To achieve this, we monitor the S_{12} interaction between two neighboring coils using the probe that plugs into the circuit board at the position of the preamplifier (see Figure 8) described in Part 6. This optimization of all next neighbors is the most time consuming adjustment procedure during phased array construction.

With a pair of coils hooked up to the network analyzer, we measure S_{12} between each adjacent pair with all other coils detuned using their active detuning circuits. We minimize S_{12} by empirically bending the crossing bridges on the loops. After each bending, the impedance of the loop is often altered, and we need to readjust the test probe to keep the 50 Ohm impedance expected by the network analyzer. We also re-adjust the tuning of the loop (variable capacitor C_3). After completing all combinations of elements, we repeated all these adjustments with a second go-thru.

Part 9: Tuning and Matching

After the geometrical decoupling, each element needs to be retuned and matched to the preamplifier's noise-matched condition. This is done using a direct S_{11} measurement with cables directly connected to the preamplifier sockets of the element under test. It is important that the electrical delay produced by the probe is accurately calibrated. When adjusting the tuning and matching all other unused elements of the phased-array are detuned. This procedure is done with the array loaded with a tightly fitted head-shaped phantom.

Part 9: Final Bench Touch Up

The final step of phased-array construction is a careful check up of the loop tuning, active detuning, and preamplifier decoupling. This step is done with all of the preamplifiers present and the array plugged into a simulator that passes the PIN diode biases and DC power to each preamplifier from the scanner. Starting with all of the array elements in the detuned states (i.e. all PIN diode bias set to forward bias the diode in each element), the bias voltage for a given loop was toggled on and off while the detuning is monitored using a double inductive probe and the S_{12} measurement (see again Figure 6). A fine adjusting of the detuning inductor is sometimes needed to achieve this. After this step, we verify the preamplifier decoupling by viewing the S_{12} versus frequency for the coil in the tuned state using the same decoupled double probe, but with reduced power output from the network analyzer (-25dBm). It is important that the minimum of the S_{21} "dip" is at the Larmor frequency (Figure 8). Note, that this measurement requires that the preamplifier is powered on. Finally the cable traps on each plug were checked and adjusted via an S_{12} measurement using current probes (Figure 9).

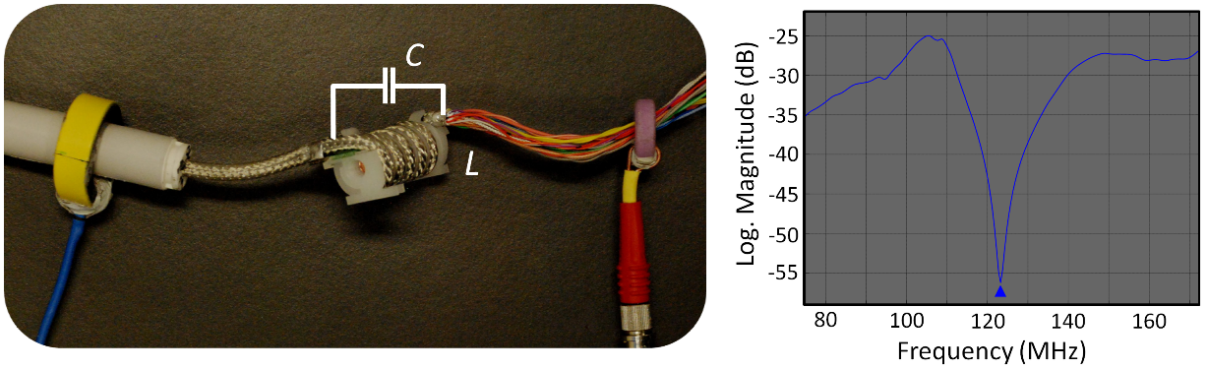

Figure 9: Adjustment of a cable trap using current injection probes. All multi core cables for each plug comprising common mode cable traps to suppress common mode currents induced by the body coil. The cable is coiled up and bridged with capacitor on the outer shield. This forms a parallel LC circuit and presents a high impedance for common mode currents. Under S_{21} recording the trap LC circuit is adjusted to minimize current flow at the Larmor frequency.

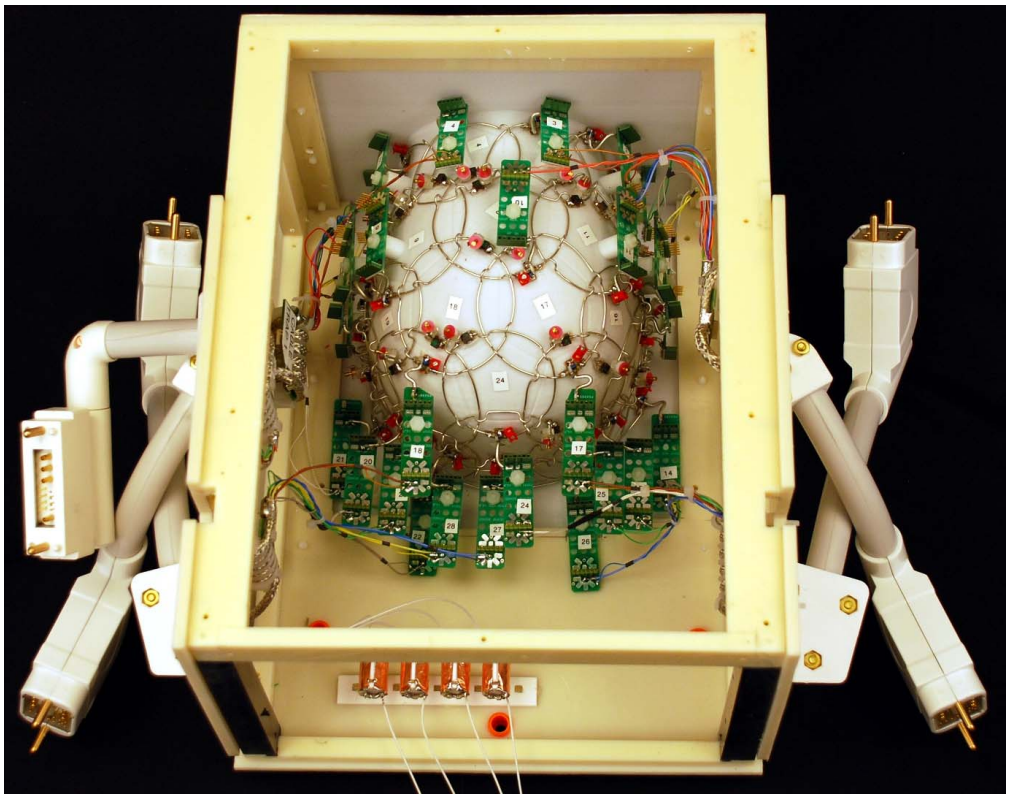

Figure 10: Assembled 32-channel coil array with five standard coil plugs to connect the constructed prototype array to the MR-scanner.

Materials:

Customized Bench Tools:

Handcrafted RF probes are commonly used in MRI coil construction. The most popular probe at the bench is the "double probe" (Figure 11a)., which is used at almost every stage of array coil construction. The probe consists of two overlapped loops made out of semi-rigid coax cable with a gap in the shield placed symmetrically in the middle of each loop. The decoupling of both loops should be >70dB. Single magnetic field probes in different sizes are also useful for various applications (Figure 11b). The small "sniffer" probe is useful to sniff out sources of resonances in circuits (e.g. isolated detuning traps). It consists of a small solenoid coil attached to the end of a coax cable (Figure 11c). Current probes are used for adjustments of common mode current traps. They are made out of a ferrite core and a single turn semi-rigid coax cable (including shield gap) (Figure 11d). For good accessibility in various measurement situations, it is helpful to have the possibility for opening up the current probe.

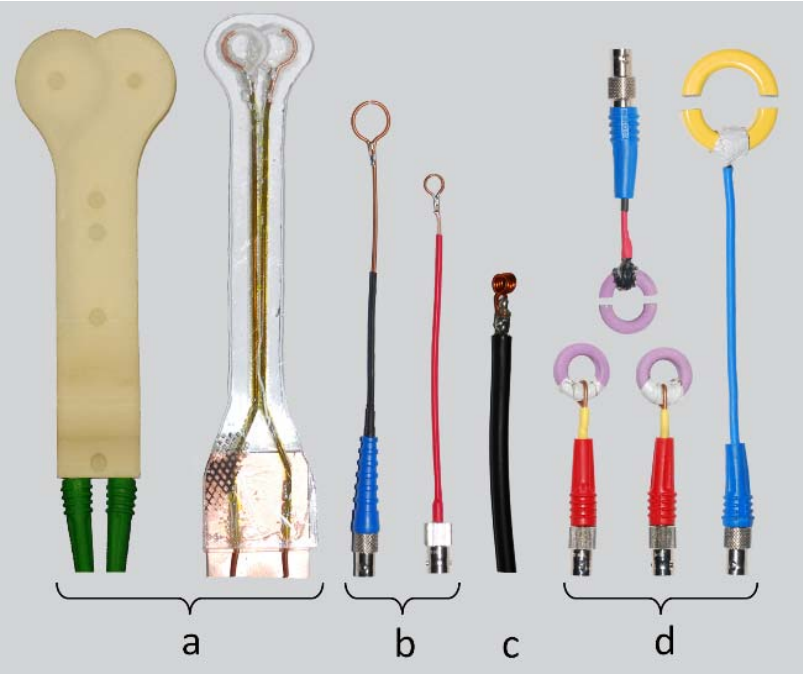

Figure 11: Handcrafted RF probes used for coil construction: (**a**) double probes, (**b**) single magnetic field probes, (**c**) sniffer probe, (**d**) current injection probes.

Non-Magnetic RF Components:

Item Description	Model / Number	Company
Non-Magnetic Chip Capacitors	Series 11	Voltronics, Corp., Danville, NJ, USA
Non-Magnetic Variable Inductor	165-02A06	Coilcraft, Inc., Cary, IL,USA
Non-Magnetic Variable Capacitor	BFC5 808 11339	Vishay Intertechnology, Inc., Malvern, USA
PIN-Diodes	MA4P4002B-402	M/A-COM Technology Solutions Inc., Lowell, MA, USA
Formable Coaxial Cable	UT-85C-FROM,	Micro-Coax, Pottstown, PA,USA

References:

[1] B. Keil, L. L. Wald, Massively Parallel MRI Detector Arrays, J. Magn. Reson. (2013) [Epub ahead of print].

[2] G. C. Wiggins, J. R. Polimeni, A. Potthast, M. Schmitt, V. Alagappan, L. L. Wald, 96-Channel receive-only head coil for 3 Tesla: design optimization and evaluation, Magn. Reson. Med. 62 (2009) 754–762.

[3] B. Keil, J. N. Blau, S. Biber, P. Hoecht, V. Tountcheva, K. Setsompop, C. Triantafyllou, L. L. Wald, A 64-channel 3T array coil for accelerated brain MRI, Magn. Reson. Med. (2012) . doi: 10.1002/mrm.24427. [Epub ahead of print].

[4] M. Schmitt, A. Potthast, D. E. Sosnovik, J. R. Polimeni, G. C. Wiggins, C. Triantafyllou, L. L. Wald, A 128-channel receive-only cardiac coil for highly accelerated cardiac MRI at 3 Tesla, Magn. Reson. Med. 59 (2008) 1431–1439.

[5] C. J. Hardy, R. O. Giaquinto, J. E. Piel, K. W. Rohling, L. Marinelli, D. J. Blezek, E. W. Fiveland, R. D. Darrow, T. K. F. Foo, 128-channel body MRI with a flexible high-density receiver-coil array, J. Magn. Reson. Imaging 28 (2008) 1219–1225.

[6] B. Keil, V. Alagappan, A. Mareyam, J. A. McNab, K. Fujimoto, V. Tountcheva, C. Triantafyllou, D. D. Dilks, N. Kanwisher, W. Lin, P. E. Grant, L. L. Wald, Size-optimized 32-channel brain arrays for 3 T pediatric imaging, Magn. Reson. Med. 66 (2011) 1777–1787.

[7] G. C. Wiggins, C. Triantafyllou, A. Potthast, A. Reykowski, M. Nittka, L. L. Wald, 32-channel 3 Tesla receive-only phased-array head coil with soccer-ball element geometry, Magn. Reson. Med. 56 (2006) 216–223.

[8] M. Hergt, R. Oppelt, M. D. Vester, A. Reykowski, K. M. Huber, K. Jahns, H. J. Fischer, Low noise preamplifier with integrated cable trap, Proceedings of the 15th Annual Meeting of ISMRM, Berlin, (2007) p. 1037.

[9] A. Kumar, W. A. Edelstein, P. A. Bottomley, Noise figure limits for circular loop MR coils, Magn. Reson. Med. 61 (2009) 1201–1209.

[10] P. B. Roemer, W. A. Edelstein, C. E. Hayes, S. P. Souza, O. M. Mueller, The NMR phased array, Magn. Reson. Med. 16 (1990) 192–225.

[11] A. Reykowski, S. M. Wright, J. R. Porter, Design of matching networks for low noise preamplifiers, Magn. Reson. Med. 33 (1995) 848–852.

[12] J. S. Hyde, A. Jesmanowicz, W. Froncisz, J. B. Kneeland, T. M. Grist, N. F. Campagna, Parallel image acquisition from noninteracting local coils, J. Magn. Reson. 70 (1986) 512–517.

[13] C. Possanzini, M. Bouteljie, Influence of magnetic field on preamplifiers using GaAs FET technology, Proceedings of the 16th Annual Meeting of ISMRM, Toronto, (2008) p. 1123.

[14] D. I. Hoult, G. Kolansky, A Magnetic-Field-Tolerant Low-Noise SiGe Pre-amplifier and T/R Switch, Proceedings of the 18th Annual Meeting of ISMRM, Stockholm, (2010) p. 649.

[15] R. Lagore, B. Roberts, B. G. Fallone, N. De Zanche, Comparison of Three Preamplifier Technologies: Variation of Input Impedance and Noise Figure With B0 Field Strength, Proceedings of the 19th Annual Meeting of ISMRM, Montreal, (2011) p. 1864.